Flow Curve Analysis of 17-4 PH Stainless Steel under Hot Compression Test

HAMED MIRZADEH, ABBAS NAJAFIZADEH, and MOHAMMAD MOAZENY

The hot compression behavior of a 17-4 PH stainless steel (AISI 630) has been investigated at temperatures of 950 °C to 1150 °C and strain rates of 10^{-3} to 10 s^{-1}. Glass powder in the Rastegaev reservoirs of the specimen was used as a lubricant material. A step-by-step procedure for data analysis in the hot compression test was given. The work hardening rate analysis was performed to reveal if dynamic recrystallization (DRX) occurred. Many samples exhibited typical DRX stress-strain curves with a single peak stress followed by a gradual fall toward the steady-state stress. At low Zener–Hollomon (Z) parameter, this material showed a new DRX flow behavior, which was called multiple transient steady state (MTSS). At high Z, as a result of adiabatic deformation heating, a drop in flow stress was observed. The general constitutive equations were used to determine the hot working constants of this material. Moreover, after a critical discussion, the deformation activation energy of 17-4 PH stainless steel was determined as 337 kJ/mol.

DOI: 10.1007/s11661-009-0029-5

I. INTRODUCTION

PRECIPITATION hardening (PH) stainless steels such as 17-4 PH, 17-7 PH, and PH 13-8 Mo are indispensable materials in many critical applications. 17-4 PH (AISI 630) is more common than any other type of PH stainless steel. Its ability to develop very high strength without the catastrophic loss of ductility and its superior corrosion resistance to other steels of similar strength have made it very attractive to engineers.[1,2] Despite the extensive work carried out on some aspects of 17-4 PH stainless steel,[2–11] very few studies have been reported on high-temperature deformation of this alloy.[12,13]

The martensitic PH stainless steels such as 17-4 PH are used in aerospace, chemical, petrochemical, and food processing applications and commonly viewed as bar alloys. Industrial hot deformation processing such as forging for these steels is conducted in the temperature range of stability of austenite phase.[12–14] Due to low stacking fault energy of austenite in the 17-4 PH stainless steel, the major restoration process during hot deformation is dynamic recrystallization (DRX). Determination of hot flow behavior and deformation resistance is quite important for successful production of this steel in accordance with aerospace specifications.[15] In our literature survey, no information was found on hot working characteristics of this important engineering alloy.

This article reports the results of the study on the hot working behavior of 17-4 PH stainless steel during the hot compression test. Moreover, a step-by-step procedure for data analysis in the hot compression test was given, and also, the general constitutive equations were used to determine the hot working constants of this material.

II. EXPERIMENTAL MATERIALS AND PROCEDURES

A. *Sample Preparation*

Chemical composition of the 17-4 PH stainless steel is shown in Table I. The base material was homogenized at a temperature of 1180 °C for 3 hours. The specimens with height of 10 mm and diameter of 5 mm were prepared. In order to minimize the occurrence of inhomogeneous compression due to the existence of friction between the anvils and the specimen surface, the Rastegaev design[16] was used, in which the entire end face of the specimen was machined away except for a small rim to form a reservoir, as shown in Figure 1. Subsequently, the reservoirs were filled with glass powder as a lubricant material. A thermocouple was spot welded to the longitudinal center of the specimen.

B. *Experimental Route*

The Baehr DIL-805* deformation dilatometer[17] was used for hot compression tests. The specimen was fastened between Al_2O_3 anvils in the vacuum chamber. Inductive heating and Ar gas quenching were used for thermal treatments. The specimen was austenitized at 1180 °C for 10 minutes and cooled with the rate of

*Baehr DIL-805 is a trademark of Bähr-Thermoanalyse GmbH, Hüllhorst, Germany.

HAMED MIRZADEH, Ph.D. Student, ABBAS NAJAFIZADEH, Professor, and MOHAMMAD MOAZENY, Master of Science, are with the Department of Materials Engineering, Isfahan University of Technology, Isfahan 84156-83111, Iran. Contact e-mail: h-m@gmx.com

Manuscript submitted June 3, 2009.
Article published online October 10, 2009

Table I. Chemical Composition (Weight Percent) of the Experimental 17-4 PH Stainless Steel

C	Cr	Ni	Cu	Mn	Si	Nb	Mo	V	S	P
0.03	15.14	4.53	3.4	0.6	0.54	0.25	0.19	0.05	0.02	0.02

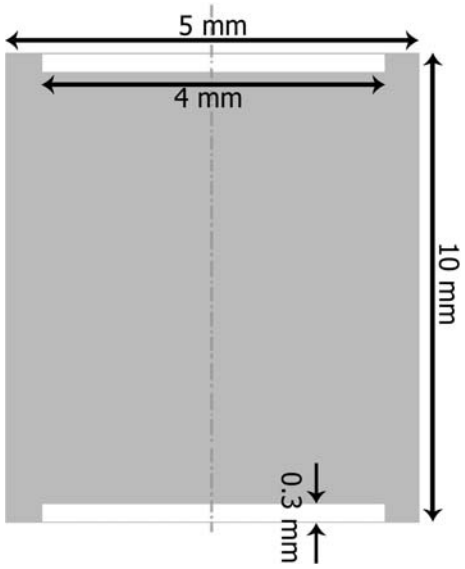

Fig. 1—Schematic of Rastegaev specimen for compression test.

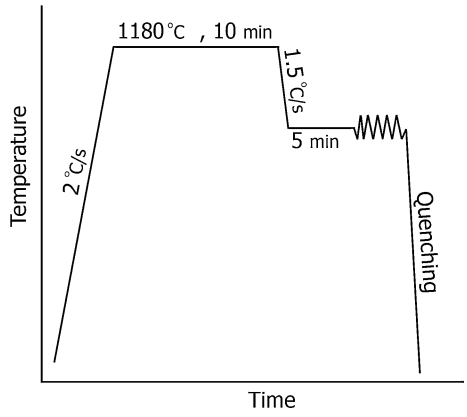

Fig. 2—Thermomechanical process used in the experiments.

1.5 °C/s to deformation temperature and held there for 5 minutes before the hot compression test. Figure 2 schematically shows the thermomechanical process used in these experiments. Single-hit hot compression tests were carried out at temperatures of 950 °C to 1150 °C with strain rates of 10^{-3} to 10 s^{-1} under a true strain of about 0.9.

C. *Remedies for Friction*

The application of suitable lubricants in the compression test may significantly reduce friction, but the lubricants are unable to eliminate it completely. Therefore, the effect of friction should be considered in the raw stress data to form the friction-corrected data. Based on the upper-bound theory, a simple theoretical analysis of the barrel compression test for determination of the constant friction factor (m) has been developed by Ebrahimi and Najafizadeh.[18] This method was used in the present study.

Table II. Calculated Friction Coefficients at Different Deformation Conditions

T	ε°	m
1150	0.001	0.11
1000	0.001	0.13
1150	0.1	0.14
1100	0.1	0.16
1150	1	0.19
1100	1	0.20
1000	0.1	0.22
1150	10	0.25
950	0.1	0.23
1000	1	0.24
950	1	0.25
1000	10	0.27

D. *Data Smoothing by Curve Fitting*

The occurrence of DRX is traditionally identified from the presence of stress peaks in flow curves. However, not all materials display well-defined peaks when tested under hot working conditions. It has been shown by Ryan and McQueen[19] and Poliak and Jonas[20–22] that the onset of DRX can also be detected from inflections in plots of the strain hardening rate against stress. The method of determining critical stress for initiation of DRX was subsequently simplified by Najafizadeh and Jonas.[23] It has been shown that this technique can be used to establish the occurrence of DRX when this cannot be determined unambiguously from the shape of the flow curve.[20–23] The derivative of the true stress with respect to true strain yields the work hardening rate, θ. Therefore, this technique requires the differentiation of the stress-strain curve, but short-range noise can render such differentiation calculus impossible. In order to solve this problem, the smoothing by fitting a high-order polynomial to flow curves was used to eliminate the irregularities and fluctuations in the experimental curves.[21,24]

In the present study, the yield or initial stress (σ_0) was first identified on each flow curve using the 0.2 pct offset method. After removal of the elastic portion,[24] each curve was corrected for friction and then was fitted and smoothed with a seventh- to ninth-order polynomial.

III. RESULTS AND DISCUSSION

A. *Friction Corrected Curves*

Table II shows the summary of friction-correction calculations. As can be seen in this table, by decreasing the deformation temperature and increasing the strain rate, the friction becomes more effective. Therefore, its

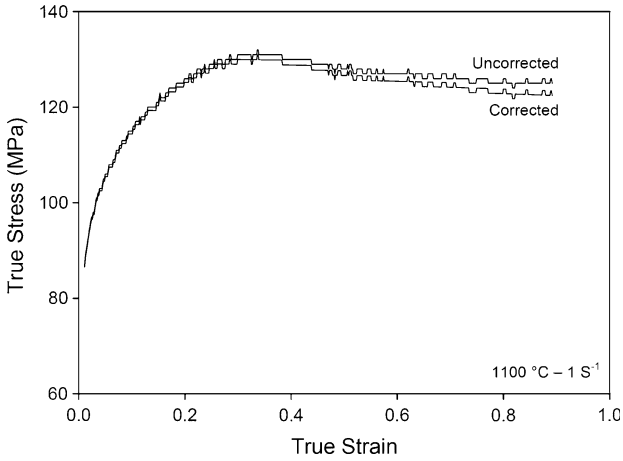

Fig. 3—Friction-corrected curve *vs* uncorrected curve at the temperature of 1100 °C and strain rate of 1 s^{-1}.

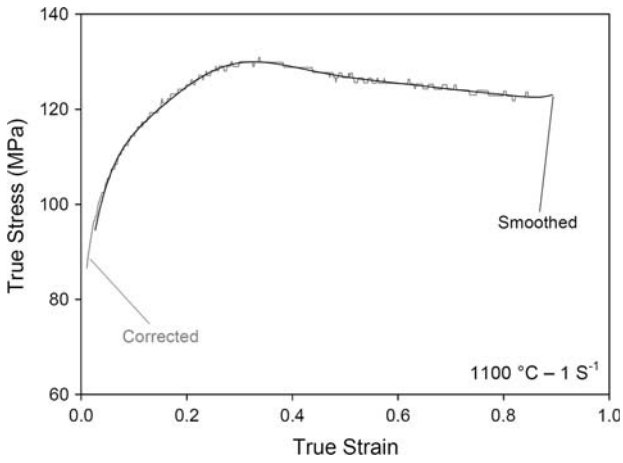

Fig. 4—Smoothed curve *vs* friction-corrected curve at the temperature of 1100 °C and strain rate of 1 s^{-1}.

effect should be considered in order to find valid stress values. An example of friction-corrected curves is shown in Figure 3. It can be seen that the effect of friction is more pronounced at higher strain values. This effect may be ignored in the flow curves up to peak; however, the effect of friction is significant after the peak point and should be taken into account.

B. *Smoothed Flow Curves*

Each curve was fitted and smoothed with a seventh- to ninth-order polynomial. Figure 4 shows a smoothed curve *vs* friction-corrected curve for the sample compressed at the temperature of 1100 °C with a strain rate of 1 s^{-1}. The fitting is pretty good. A number of smoothed flow curves obtained for different temperatures and strain rates are also shown in Figure 5. Many samples exhibit typical DRX flow curves with a single peak stress followed by a gradual fall toward the steady-state stress.

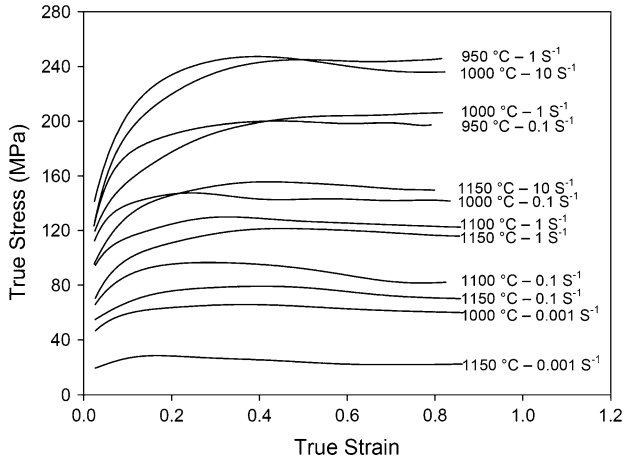

Fig. 5—Smoothed flow curves obtained for different deformation conditions.

If stress oscillations appear before reaching the steady state, then several recrystallization and grain growth cycles occur and the stress behavior is said to be of the cyclic or multiple peak type. The particular stress behavior before reaching the steady state depends on the initial grain size, temperature, and strain rate.[25–28] However, there is no evidence of classical multiple peaks in the flow curves of this work, even at a very low strain rate of 0.001 s^{-1} and high temperature of 1150 °C.

Close views of the original flow curves in the case of T = 1100 °C with ε° = 1 s^{-1} and T = 1150 °C with ε° = 0.001 s^{-1} are shown in Figures 6(a) and (b), respectively. The flow curve of Figure 6(a) represents the classical single peak behavior. However, Figure 6(b) represents a strange behavior, neither the single peak behavior nor the conventional cyclic behavior. Several plateaus (horizontal stress line) followed by a decrease in flow stress after each plateau are detected beyond the peak point of its flow curves. Each plateau represents a transient steady-state period (similar to a peak point), and the decrease in flow stress after each plateau may be attributed to the progress of a new DRX cycle. This condition may be considered as a transition state between single and multiple peak behaviors, which was called multiple transient steady state (MTSS).

In the case of single peak behavior (Figure 7(a)), new cycles of DRX initiate before completion of the first cycle. Therefore, different grains will be at different stages of the DRX process at any point of time. The flow curve will represent the averaged flow stress of grains at different stages of recrystallization in the form of a single peak curve. In the case of multiple peak behavior (Figure 7(b)), several successive cycles of DRX occurred before the steady-state strain, which result in multiple peak behavior. However, in the case of the present investigation, there may be an overlap between the end of a given cycle and the onset of the subsequent cycle of DRX (Figure 7(c)). At the last stages of a cycle, the rate of restoration by the recrystallization process is relatively low and the material work hardened under

deformation. At the same time, the rate of the new DRX cycle increases. Therefore, probably due to the simultaneous effect of work hardening at the last stages of the old DRX cycle and flow softening by initiation of the new DRX cycle, the stress rise after each stress minimum did not occur and the multiple transient steady-state behavior was produced. This is an interesting aspect that has not been reported elsewhere.

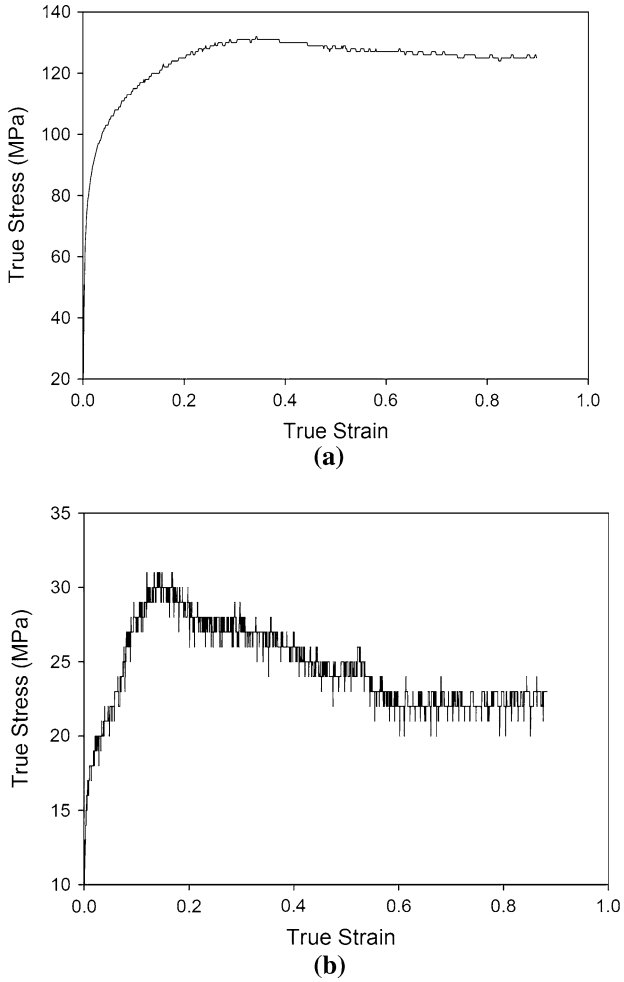

Fig. 6—Close view of the original flow curves: (*a*) 1100 °C–1 s^{-1} and (*b*) 1150 °C–0.001 s^{-1}.

As can be seen in Figure 5, the peak becomes less obvious with increasing strain rate and decreasing temperature. At deformation conditions of 1000 °C–1 s^{-1} and 950 °C–1 s^{-1}, the shape of flow curves resembles typical dynamic recovery (DRV) behavior. However, inflections in θ-σ plots are considered as stronger indications of the occurrence of DRX.[21] Therefore, the θ-σ analysis and microstructural investigations were performed to reveal whether DRX occurred.

C. *Work Hardening Rate Analysis*

In this work, the occurrence of DRX was detected from the inflection in the plot of θ against σ up to the peak point of the stress-strain curve. In some problematic cases, the minimum in the plot of $-d\theta/d\sigma$ *vs* σ was considered for this purpose. The θ values were obtained using the central difference approach[2] by the following equation:

$$\theta|_i = \left.\frac{d\sigma}{d\varepsilon}\right|_i = \frac{\sigma|_{i+1} - \sigma|_{i-1}}{\varepsilon_{i+1} - \varepsilon_{i-1}} \qquad [1]$$

A number of θ-σ curves are shown in Figure 8. In each curve, θ linearly decreases with the flow stress. After that, the curves gradually change to a lower slope and then drop toward $\theta = 0$ at peak stress. This figure also shows that the $T = 1000$ °C with $\varepsilon^\circ = 1\ s^{-1}$ and $T = 950$ °C with $\varepsilon^\circ = 1\ s^{-1}$ conditions, despite the shape of their flow curves, have a clear inflection point that indicates the occurrence of DRX in these cases.

At the deformation condition of $T = 1000$ °C with $\varepsilon^\circ = 10\ s^{-1}$, the shape of the flow curve represents the occurrence of extensive DRX, but neither an inflection point nor a minimum were determined on the θ-σ and $-d\theta/d\sigma$-σ curves, respectively. The softening beyond the peak may be attributed to adiabatic deformation

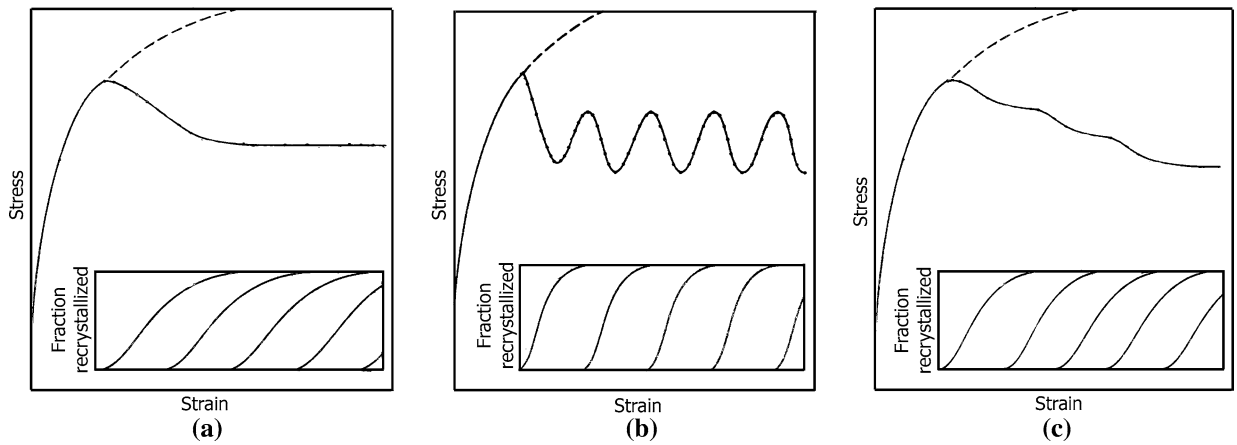

Fig. 7—Schematic representation of (*a*) single peak, (*b*) multiple peaks, and (*c*) MTSS.

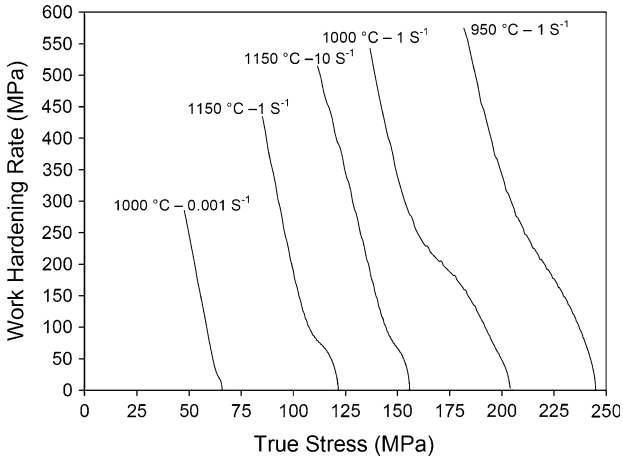

Fig. 8—Strain hardening rate *vs* flow stress.

heating[29] or, in some cases, localization of strain or sample failure.[30] However, at a high strain rate of 10 s^{-1}, the effect of adiabatic heating seems to be significant. Figure 9(a) represents the stress and the temperature in terms of strain for this sample. The figure clearly shows that the temperature rise due to adiabatic heating after the peak point is sufficiently high. Therefore, the flow stress of the sample was reduced due to increasing its temperature. Similar figures at $T = 1000$ °C with $\varepsilon^\circ = 1$ s^{-1} and $T = 1000$ °C with $\varepsilon^\circ = 0.001$ s^{-1} are shown in Figures 9(b) and (c), respectively. It can be seen that the deformation heating in these cases is negligible or has an arbitrary profile.

The microstructures of samples deformed at $T = 1000$ °C with $\varepsilon^\circ = 10$ s^{-1} and at $T = 1150$ °C with $\varepsilon^\circ = 10$ s^{-1} are shown in Figure 10. As can be seen in Figure 10(a), the 1150 °C–10 s^{-1} condition shows the nearly complete DRX structure that was expected from the shape of its flow curve (Figure 5). However, by decreasing the deformation temperature up to 1000 °C at the same strain rate of 10 s^{-1}, the pancake structure has been produced (Figure 10(b)).

D. *Constitutive Equations*

Constitutive equations are commonly used to calculate the flow stress of a material during deformation. The base equation is shown in Eq. [2]. In this equation, the Zener–Hollomon parameter (Z) is the temperature-compensated strain rate and Q is the activation energy of deformation.

$$Z = \varepsilon^\circ \exp\left(\frac{Q}{RT}\right) = f(\sigma) \qquad [2]$$

In constitutive equations, the Z parameter may be considered as a function of stress (Eq. [2]). The power-law description of stress (Eq. [3]) is preferred for creep, but it cannot be used when stresses are high. Conversely, the exponential law (Eq. [4]) is only suitable for relatively low temperatures and high strain rates.

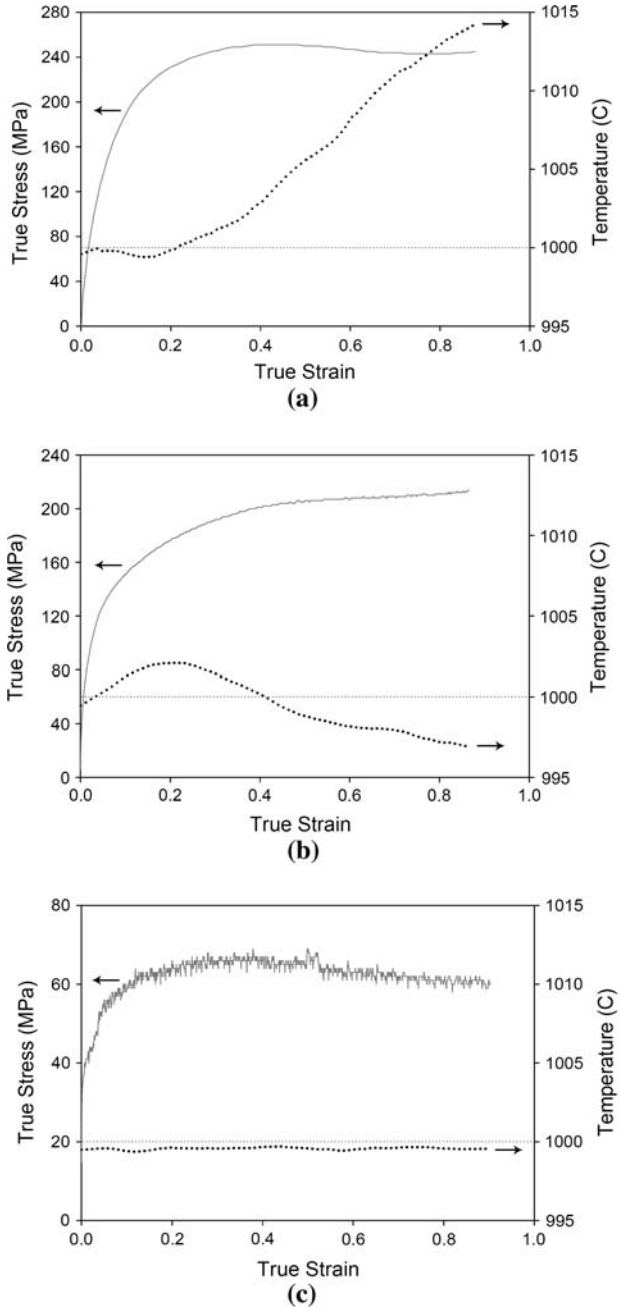

Fig. 9—Stress and temperature in terms of strain for samples deformed at (*a*) 1000 °C–10 s^{-1}, (*b*) 1000 °C–1 s^{-1}, and (*c*) 1000 °C–0.001 s^{-1}.

However, the hyperbolic sine law (Eq. [5]) can be used for a wide range of temperatures and strain rates:[31,32]

$$Z = f(\sigma) = A'\sigma^{n'} \qquad [3]$$

$$Z = f(\sigma) = A'' \exp(\beta\sigma) \qquad [4]$$

$$Z = f(\sigma) = A[\sinh(\alpha\sigma)]^n \qquad [5]$$

where A', A'', A, n', n, β, and $\alpha(\approx\beta/n')$ are material constants. The stress multiplier α is an adjustable

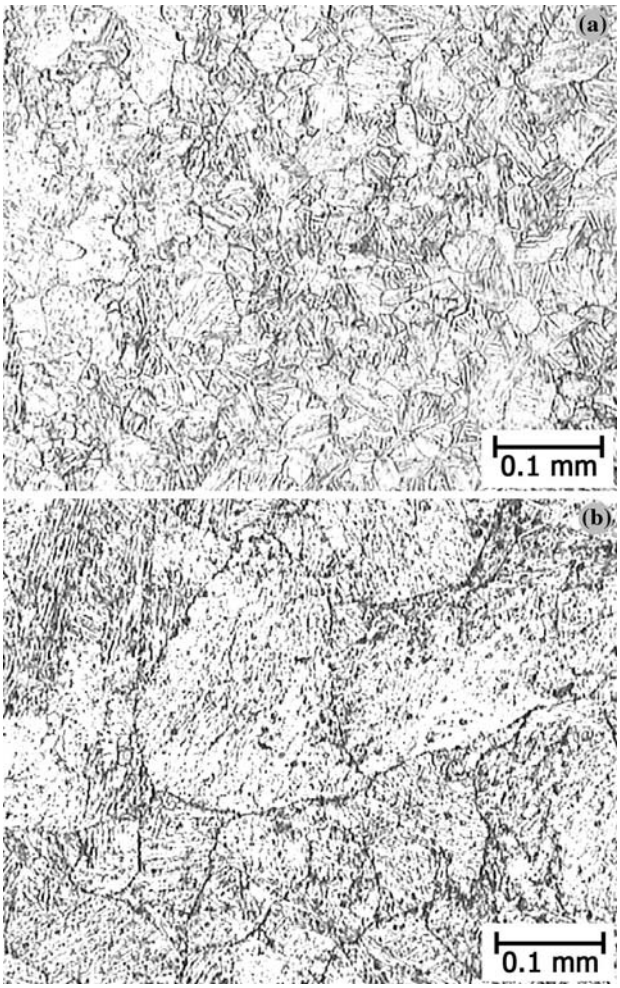

Fig. 10—Microstructure of samples deformed at (*a*) 1150 °C–10 s^{-1} and (*b*) 1000 °C–10 s^{-1} (etched with Superpicral to reveal the prior austenite grain boundaries).

constant that brings $\alpha\sigma$ into the correct range to make constant T curves in $\ln \varepsilon^{\circ}$ *vs* $\ln\{\sinh(\alpha\sigma)\}$ plots linear and parallel.[33]

In these equations, the flow stress is related to both the absolute temperature during deformation and to strain rate. However, the description of flow stress by these equations is incomplete, because no strain for determination of flow stress is specified. Therefore, characteristic stresses such as steady state, peak, or the one corresponding to a specific strain may be used for this purpose.[34,35] Since the steady-state stress may not be precisely attained or there may be some softening due to morphological evolution, it is usual to use the peak stress.[33] Many research results indicated that the peak and the steady-state stresses have linear relation.[36] On the other hand, peak stress is more important for industrial processes.

E. *Determination of Hot Working Constants*

By substitution of $f(\sigma)$ from Eqs. [3], [4], and [5] to Eq. [2], and taking the natural logarithm from each side of the resulting equations, the following expressions could be derived for peak stress:

$$\ln \varepsilon^{\circ} + \frac{Q}{R}(1/T) = \ln A' + n' \ln \sigma_P \quad [6]$$

$$\ln \varepsilon^{\circ} + \frac{Q}{R}(1/T) = \ln A'' + \beta \sigma_P \quad [7]$$

$$\ln \varepsilon^{\circ} + \frac{Q}{R}(1/T) = \ln A + n \ln\{\sinh(\alpha\sigma_P)\} \quad [8]$$

At constant deformation temperature, partial differentiation of Eqs. [6], [7], and [8] yields the following equations, respectively:

$$n' = [\partial \ln \varepsilon^{\circ} / \partial \ln \sigma_P]_T \quad [9]$$

$$\beta = [\partial \ln \varepsilon^{\circ} / \partial \sigma_P]_T \quad [10]$$

$$n = [\partial \ln \varepsilon^{\circ} / \partial \ln\{\sinh(\alpha\sigma_P)\}]_T \quad [11]$$

It follows from these expressions that the slope of the plot of $\ln \varepsilon^{\circ}$ against $\ln \sigma_P$ and the slope of the plot of $\ln \varepsilon^{\circ}$ against σ_P can be used for obtaining the values of n' and β, respectively. These plots are shown in Figures 11(a) and (b). The linear regression of these data results in the average values of 5.627 and 0.061 for n' and β, respectively. This gives the value of $\alpha = \beta / n' = 0.011$. According to Eq. [11], the slope of the plot of $\ln \varepsilon^{\circ}$ against $\ln\{\sinh(\alpha\sigma_P)\}$ can be used for obtaining the value of n (Figure 11(c)). The average value of n was determined as 4.17.

F. *Activation Energy of Hot Working*

Since the Zener–Hollomon parameter is extensively used in hot working, calculating the correct value of deformation activation energy (Q) is essential. There are many ways to fit the data for this calculation. Some of them may lead to significant errors, as shown in the following.

At a constant strain rate, partial differentiation of Eqs. [6], [7], and [8] yields the following equations, respectively:

$$Q = Rn'[\partial \ln \sigma_P / \partial(1/T)]_{\varepsilon^{\circ}} \quad [12]$$

$$Q = R\beta[\partial \sigma_P / \partial(1/T)]_{\varepsilon^{\circ}} \quad [13]$$

$$Q = Rn[\partial \ln \sinh(\alpha\sigma_P) / \partial(1/T)]_{\varepsilon^{\circ}} \quad [14]$$

It follows from these expressions that the slope of the plots of $\ln \sigma_P$, σ_P, or $\ln \sinh(\alpha\sigma_P)$ against the reciprocal of absolute temperature can be used for obtaining the value of Q. These plots are shown in Figure 12. The linear regression of these data results in the average values of 337, 543, and 442 kJ/mol for activation energy from Eqs. [12], [13], and [14], respectively.

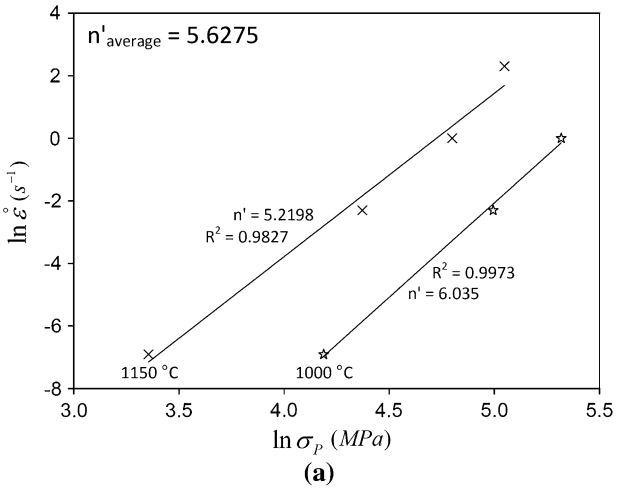

(a)

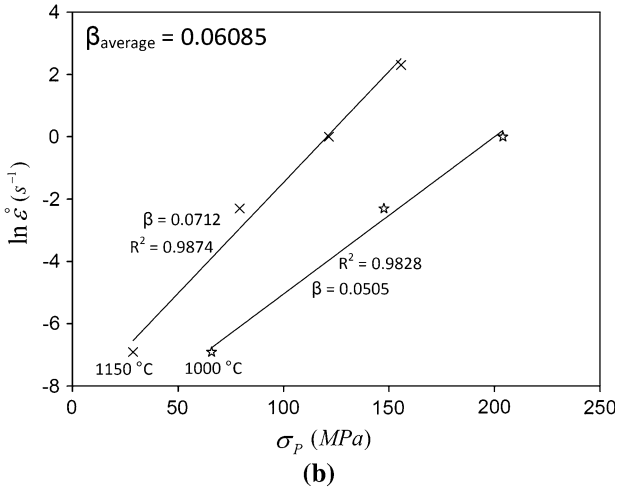

(b)

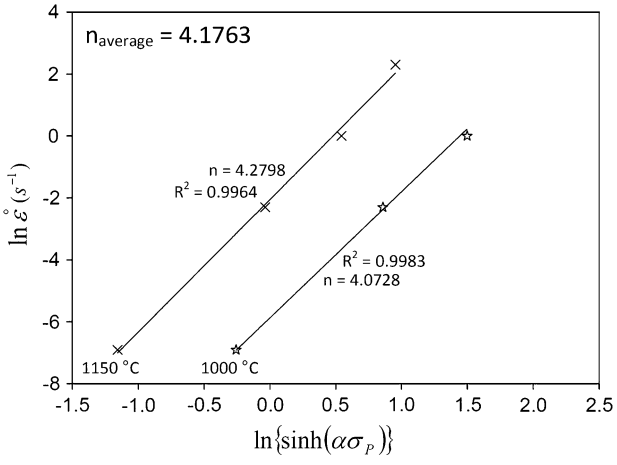

(c)

Fig. 11—Plots used for calculation of (*a*) *n*′, (*b*) *β*, and (*c*) *n*.

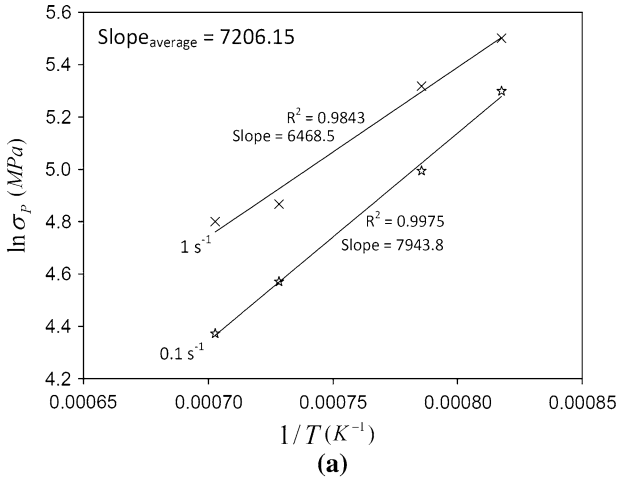

(a)

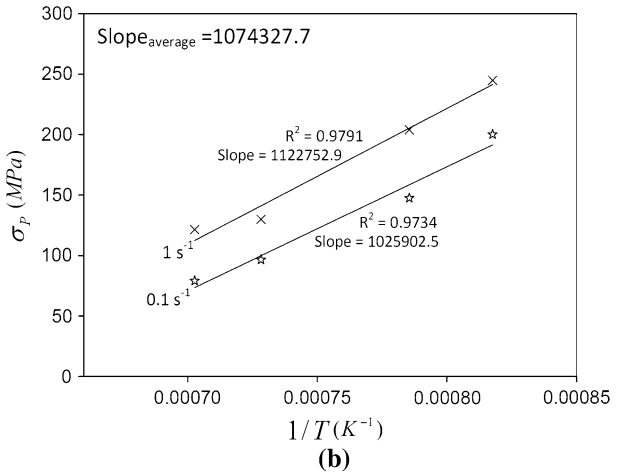

(b)

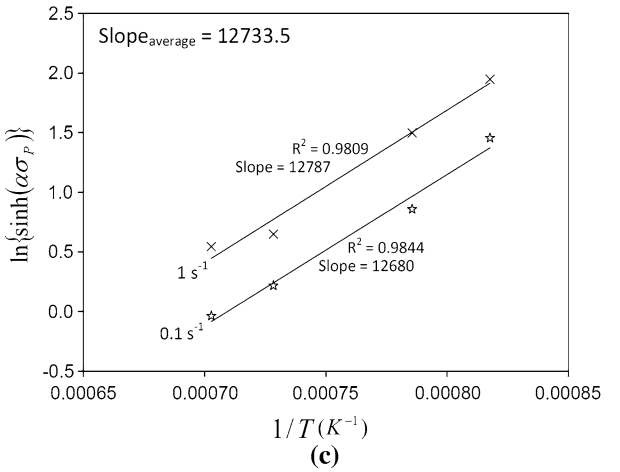

(c)

Fig. 12—Plots of (*a*) ln σ_P, (*b*) σ_P, and (*c*) ln sinh($\alpha\sigma_P$) against the reciprocal of absolute temperature.

There is a significant difference between these values. Analysis of the correlation coefficient (R^2) of these regression values reveals that Eq. [12] has better fit to experimental data. Therefore, the activation energy of hot working was considered to be 337 kJ/mol. Since the 17-4 PH stainless steel is austenitic at the hot working condition, this behavior can be compared to a similar austenitic stainless steel with the same level of alloying elements. For such an austenitic stainless steel, the value of 337 kJ/mol is reasonable.[33] So, in general, for calculation of the activation energy of hot working,

one of the three expressions of $f(\sigma)$ results in the appropriate value.

G. *Peak Stress as a Function of the Zener–Hollomon Parameter*

According to Eqs. [3] through [5], the plots of ln Z *vs* ln σ_P, σ_P, and ln{sinh($\alpha\sigma$)} may be used to find the relationship between Z and σ_P. The corresponding curves are shown in Figure 13, and the resultant regression equations with new constants are as follows:

$$Z = \varepsilon^{\circ} \exp\left(\frac{337 \times 10^3}{RT}\right) = 10 \times \sigma_P^{5.52} \qquad [15]$$

$$Z = \varepsilon^{\circ} \exp\left(\frac{337 \times 10^3}{RT}\right) = 3.3 \times 10^9 \times \exp(0.0496 \times \sigma_P) \qquad [16]$$

$$Z = \varepsilon^{\circ} \exp\left(\frac{337 \times 10^3}{RT}\right) = 2.64 \times 10^{11} \times [\sinh(0.011 \times \sigma_P)]^{3.73} \qquad [17]$$

Among these relations, the power equation (Eq. [15]) not only has the highest correlation coefficient, but also is simple and easy to use. The hyperbolic sine law also has a good fit. The hyperbolic sine law yields to the power and the exponential laws in low and high stresses, respectively. Therefore, it is suitable for analysis over a wide range of temperatures and strain rates. Conversely, the exponential equation is inappropriate to express hot working characteristics in the case of the present investigation. In summary, the peak stress of 17-4 PH stainless steel under the deformation condition used in this work may be expressed as Eq. [18] as a result of rearrangement of Eq. [15].

$$\sigma_P = 0.66 \times Z^{0.18} \qquad [18]$$

IV. CONCLUSIONS

A step-by-step data analysis of flow curves of 17-4 PH stainless steel resulted in the following principal conclusions:

1. At a low Zener–Hollomon parameter (Z), this material showed a new DRX flow behavior, which was called MTSS, whereas at high Z, a drop in flow stress was observed that depends on the adiabatic deformation heating. At medium Z values, the stress-strain curves exhibited typical DRX behavior with a single peak stress followed by a gradual fall toward a steady-state stress.
2. Although some samples exhibited typical DRV or DRX behavior, the inflection analysis in the work hardening rate *vs* stress plots proved the occurrence of DRX or DRV, respectively.

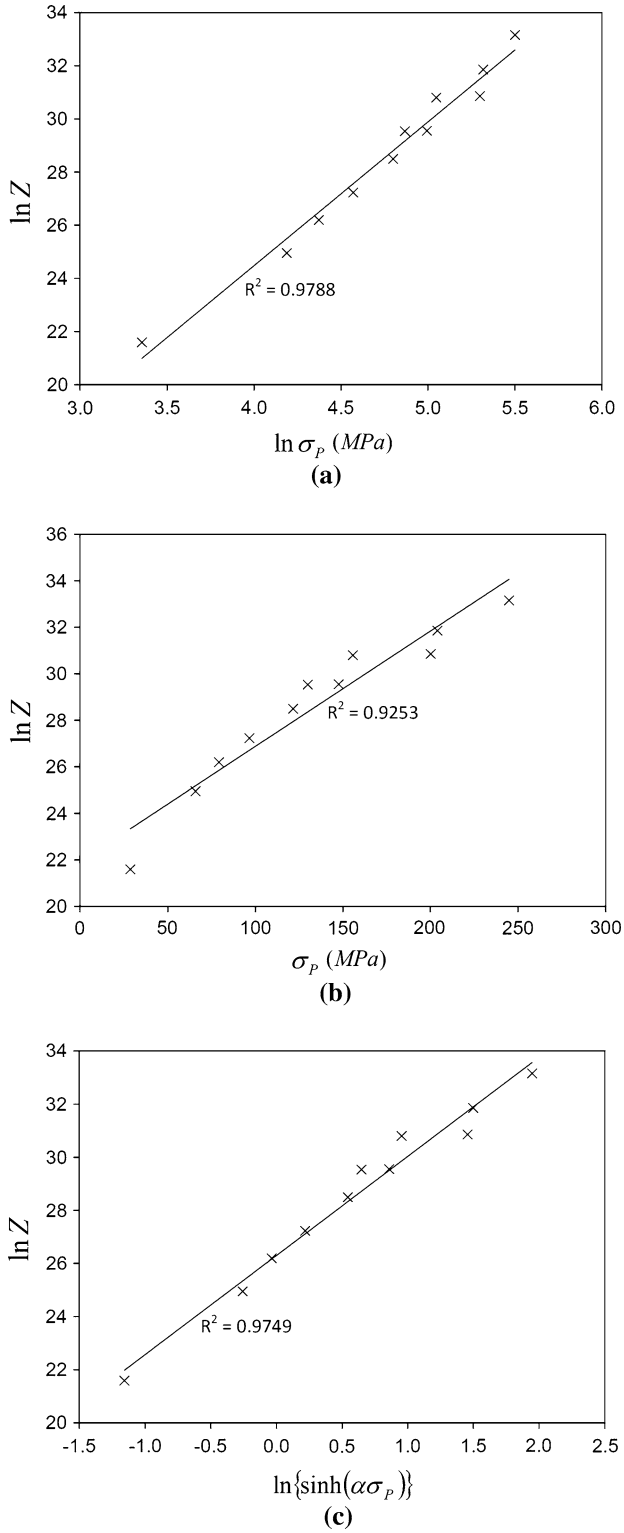

Fig. 13—Plots of ln Z *vs* (*a*) ln σ_P, (*b*) σ_P, and (*c*) ln sinh($\alpha\sigma_P$).

3. It was shown that for correct calculation of the activation energy of hot working, one of the three expressions of Z, namely, the power law, exponential law, and hyperbolic sine law, results in the appropriate value. For 17-4 PH stainless steel, the

power law was found to be the appropriate relation, which resulted in the value of 337 kJ/mol.

REFERENCES

1. R.A. Lula: *Stainless Steel*, ASM, Metals Park, OH, 1986, pp. 80–86.
2. H. Mirzadeh and A. Najafizadeh: *Mater. Chem. Phys.*, 2009, vol. 116, pp. 119–24.
3. H.J. Rack and D. Kalish: *Metall. Trans.*, 1974, vol. 5, pp. 1595–1605.
4. C.N. Hsiao, C.S. Chiou, and J.R. Yang: *Mater. Chem. Phys.*, 2002, vol. 74, pp. 134–42.
5. J. Wang, H. Zou, C. Li, S. Qiu, and B. Shen: *Mater. Charact.*, 2006, vol. 57, pp. 274–80.
6. M. Murayama, Y. Katayama, and K. Hono: *Metall. Mater. Trans. A*, 1999, vol. 30A, pp. 345–53.
7. K.C. Hsu and C.K. Lin: *Int. J. Fatigue*, 2008, vol. 30, pp. 2147–55.
8. S. Kundu, M. Ghosh, and S. Chatterjee: *Mater. Sci. Eng. A*, 2006, vol. 428, pp. 18–23.
9. L.W. Tsay, W.C. Lee, R.K. Shiue, and J.K. Wu: *Corr. Sci.*, 2002, vol. 44, pp. 2101–18.
10. M. Esfandiari and H. Dong: *Surf. Coat. Technol.*, 2007, vol. 202, pp. 466–78.
11. K.S. Raja and K. Prasad Rao: *J . Mater. Sci. Lett.*, 1993, vol. 12, pp. 957–60.
12. S. Isogawa, H. Yoshida, Y. Hosoi, and Y. Tozawa: *J. Mater. Process. Technol.*, 1998, vol. 74, pp. 298–306.
13. AK Steel, 17-4 PH-B-08-01-07, http://www.aksteel.com, 2007.
14. A. Momeni, A. Shokuhfar, and S.M. Abbasi: *J. Mater. Sci. Technol.*, 2007, vol. 23, pp. 775–78.
15. Aerospace Material Specification, AMS 5643Q, SAE International, Warrendale, PA, 2003.
16. R. Herbertz and H. Wiegels: *Stahl Eisen.*, 1981, vol. 101, pp. 89–92.
17. Bähr-Thermoanalyse GmbH, http://www.baehr-thermo.de, 2008.
18. R. Ebrahimi and A. Najafizadeh: *J. Mater. Process. Technol.*, 2004, vol. 152, pp. 136–43.
19. N.D. Ryan and H.J. McQueen: *Can. Metall. Q.*, 1990, vol. 29, pp. 47–162.
20. E.I. Poliak and J.J. Jonas: *Acta Mater.*, 1996, vol. 44, pp. 127–36.
21. E.I. Poliak and J.J. Jonas: *ISIJ Int.*, 2003, vol. 43, pp. 684–91.
22. E.I. Poliak and J.J. Jonas: *ISIJ Int.*, 2003, vol. 43, pp. 692–700.
23. A. Najafizadeh and J.J. Jonas: *ISIJ Int.*, 2006, vol. 46, pp. 1679–84.
24. J.J. Jonas, X. Quelennec, L. Jiang, and E. Martin: *Acta Mater.*, 2009, vol. 57, pp. 2748–56.
25. M.J. Luton and C.M. Sellars: *Acta Metall.*, 1969, vol. 17, pp. 1033–43.
26. T. Sakai and J.J. Jonas: *Acta Metall.*, 1984, vol. 32, pp. 189–209.
27. A. Dehghan-Manshadi and P.D. Hodgson: *ISIJ Int.*, 2007, vol. 47, pp. 1799–803.
28. R.E. Reed-Hill and R. Abbaschian: *Physical Metallurgy Principles*, 3rd ed., PWS Publishing, Boston, MA, 1994, pp. 886–89.
29. M. Naderi, L. Durrenberger, A. Molinari, and W. Bleck: *Mater. Sci. Eng. A*, 2008, vol. 478, pp. 130–39.
30. A. Dehghan-Manshadi, M.R. Barnett, and P.D. Hodgson: *Mater. Sci. Eng. A*, 2008, vol. 485, pp. 664–72.
31. F.A. Slooff, J. Zhou, J. Duszczyk, and L. Katgerman: *Scripta Mater.*, 2007, vol. 57, pp. 759–62.
32. K. Lim, P.A. Manohar, D. Lee, Y.-C. Yoo, C.M. Cady, G.T. Gray, and A.D. Rollett: *Mater. Sci. Forum,* 2003, vols. 426–432, pp. 3903–08.
33. H.J. McQueen and N.D. Ryan: *Mater. Sci. Eng. A*, 2002, vol. 322, pp. 43–63.
34. H. Yang, Z.-H. Li, and Z.-L. Zhang: *J. Zhejiang Univ. Sci. A*, 2006, vol. 7, pp. 1453–60.
35. S. Mandal, V. Rakesh, P.V. Sivaprasad, S. Venugopal, and K.V. Kasiviswanathan: *Mater. Sci. Eng. A*, 2009, vol. 500, pp. 114–21.
36. T. Sakai: *J. Mater. Process. Technol.*, 1995, vol. 53, pp. 349–61.